High-Areal-Density Fuel Assembly in Direct-Drive Cryogenic Implosions

T. C. Sangster, V. N. Goncharov, P. B. Radha, V. A. Smalyuk, R. Betti, R. S. Craxton,* J. A. Delettrez, D. H. Edgell, V. Yu. Glebov, D. R. Harding, D. Jacobs-Perkins, J. P. Knauer, F. J. Marshall, R. L. McCrory,* P. W. McKenty, D. D. Meyerhofer,* S. P. Regan, W. Seka, R. W. Short, S. Skupsky, J. M. Soures, C. Stoeckl, and B. Yaakobi
Laboratory For Laser Energetics, University of Rochester, 250 East River Road, Rochester, New York 14623-1299, USA

D. Shvarts
NRCN, Beer Sheva 84190, Israel

J. A. Frenje, C. K. Li, R. D. Petrasso, and F. H. Séguin
Plasma Science and Fusion Center, Massachusetts Institute of Technology, Cambridge, Massachusetts 02139, USA
(Received 9 November 2007; published 8 May 2008)

The first observation of ignition-relevant areal-density deuterium from implosions of capsules with cryogenic fuel layers at ignition-relevant adiabats is reported. The experiments were performed on the 60-beam, 30-kJ$_{UV}$ OMEGA Laser System [T. R. Boehly *et al.*, Opt. Commun. **133**, 495 (1997)]. Neutron-averaged areal densities of 202 ± 7 mg/cm^2 and 182 ± 7 mg/cm^2 (corresponding to estimated peak fuel densities in excess of 100 g/cm^3) were inferred using an 18-kJ direct-drive pulse designed to put the converging fuel on an adiabat of 2.5. These areal densities are in good agreement with the predictions of hydrodynamic simulations indicating that the fuel adiabat can be accurately controlled under ignition-relevant conditions.

DOI: 10.1103/PhysRevLett.100.185006 PACS numbers: 52.57.−z

Inertial confinement fusion [1] of deuterium-tritium (DT) at reactor-scale facilities promises a virtually unlimited source of energy [2]. In direct-drive inertial confinement fusion [3], nominally identical laser beams symmetrically illuminate a spherical capsule containing a frozen shell of DT. Ablation of material from the surface of the capsule causes the fuel shell to implode. To achieve ignition and moderate gain using a MJ-class laser such as the National Ignition Facility (NIF) [4], the imploding shell must reach a velocity greater than $\sim 3 \times 10^7$ cm/s and the fuel areal density at maximum compression (ρR_m) must exceed ~ 1.5 g/cm^2 [5]. Detailed calculations show that, for a given laser energy E_L, ρR_m depends mainly on the in-flight fuel adiabat α (the ratio of the shell pressure to the Fermi-degenerate pressure at the shell density): $\rho R_m = 2.6[E_L(\mathrm{MJ})]^{1/3}/\alpha^{0.54}$ [6]. Therefore, the fuel pressure in a high-gain implosion (i.e., where the fusion energy released is at least 50 times E_L) driven with a laser energy of 1 MJ cannot exceed the Fermi-degenerate pressure by more than factor of ~ 3 [7]. This requires that the mechanisms leading to increases in the adiabat during the shell acceleration be properly modeled during the design of the target. Agreement between the measured and predicated areal density ensures accurate control over the adiabat during the implosion.

To validate the predicted performance of ignition-relevant target designs, a series of direct-drive cryogenic D_2 target implosions is underway [8,9] on the 60-beam, 30-kJ$_{UV}$ OMEGA laser [10]. The targets [see Fig. 1(a)] consist of 3–10-μm-thick spherical shells of deuterated plastic (CD) with a 95-μm-thick cryogenic layer of deuterium ice (the inner ice roughness is generally less than 3-μm rms in all modes [11]). The design adiabat for these experiments was systematically varied from $\alpha \sim 2$ to $\alpha \sim 25$, while the peak on-target laser intensity ranged between 0.25 and 1.5×10^{15} W/cm^2. The goal of these experiments was to demonstrate ignition-relevant fuel compression at low adiabat; the implosion velocities and in-flight aspect ratios were lower than required for a full validation of ignition-target designs.

The areal density is inferred from the energy loss of secondary protons in the dense fuel shell [12]. These protons sample an approximately 100–200-ps window of the temporal shell ρR evolution and consequently the neutron-averaged areal density ρR_n is typically less than ρR_m. For implosions with highly distorted cores, ρR_n can be significantly less than ρR_m since the perturbations cool the core and truncate the burn before the fuel reaches peak compression. Therefore, it is important to account for the burn history when comparing measured areal densities with simulations.

Recent experiments have shown that the predicted ρR_n agrees with the measured ρR_n for low-adiabat implosions driven at intensities below 3×10^{14} W/cm^2 [13]. Ignition designs driven at such low intensities would require highly unstable, large aspect ratio targets (the ratio of the fuel shell radius to its thickness) to achieve implosion velocities in excess of 3×10^7 cm/s; more robust ignition targets must therefore be driven at higher intensities. In this Letter, it is shown that ignition-relevant areal densities (i.e., a significant fraction of what is needed for alpha heating [5]) can be achieved in targets driven at an intensity of

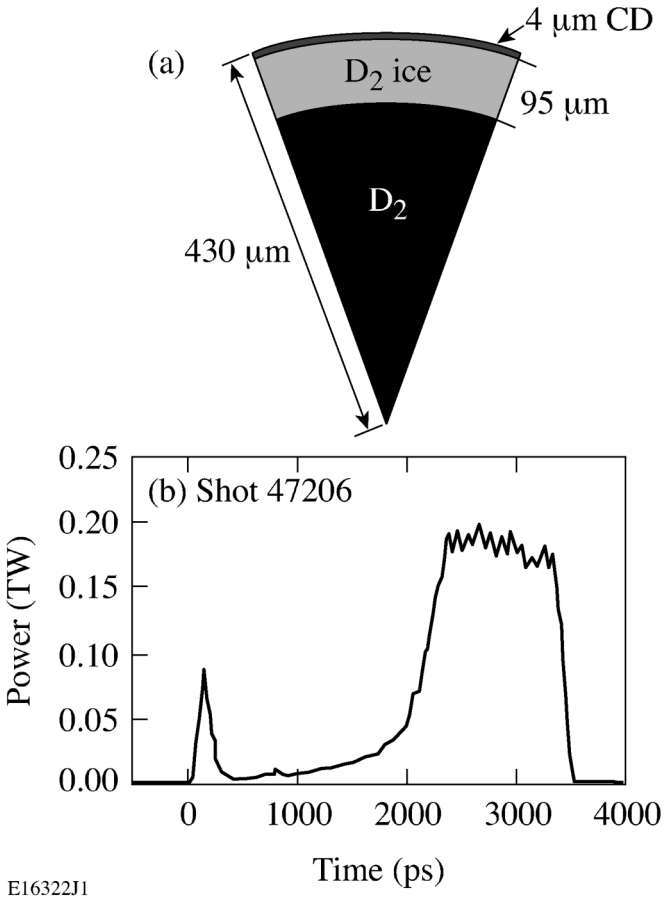

FIG. 1. (a) A typical cryogenic target consists of a thin ($\sim$ 4-μm) outer CD shell and a thick ($\sim$ 95-μm) layer of D_2 ice. (b) The temporal history of the power per beam for a low-adiabat decaying-shock-drive pulse on OMEGA.

5×10^{14} W/cm^2 when the shock velocity is adequately modeled and hot-electron preheat is mitigated.

Several processes can increase the fuel adiabat and degrade ρR_m. These include shock heating during the early stages of the implosion (due to shock mistiming), fuel preheat from energetic electrons ($T_{\text{hot}} > 50$ keV) generated by laser-driven plasma instabilities (e.g., the two-plasmon-decay [14]), and hydrodynamic instability growth leading to shell breakup during acceleration [15]. To minimize the effect of nonuniformity growth on adiabat degradation, adiabat shaping [16,17] is used as part of the overall target design; Fig. 1(b) shows a typical 18-kJ laser-drive pulse for this series of experiments.

Precise control over shock timing is required to minimize adiabat degradation caused by shock heating. The first shock wave launched by the picket in Fig. 1(b) establishes the shell adiabat. To prevent an excessive increase in the adiabat at the inner surface of the fuel shell, the coalescence of this first shock and the compression wave launched during the rise of the main drive pulse must be timed to 100 ps for the energy-scaled OMEGA designs. To meet this requirement, the laser-deposition and thermal-conduction models in the 1D radiation hydrocode LILAC [18] used to design the targets were improved based on shock breakout and velocity measurements in cryogenic D_2 [19]. In particular, a nonlocal model [20,21] was applied to simulate electron thermal conduction. This led to better agreement with the time-resolved laser energy absorbed by the target [22,23].

To reach implosion velocities greater than 3×10^7 cm/s with a robust target design, drive intensities will need to exceed 5×10^{14} W/cm^2. For a given in-flight aspect ratio A, the implosion velocity can be written as $V_{\text{imp}}^2 \sim P_a A/\rho \sim I_L^{2/3} A$. This implies that an upper limit on V_{imp} may be determined by the intensity threshold for the plasma instabilities developed near the quarter-critical density surface in the coronal plasma; the energetic electrons produced by these instabilities deposit energy throughout the fuel shell, effectively raising the fuel adiabat. As discussed by Smalyuk *et al.* [13], this hot-electron preheat is inferred by measuring the bremsstrahlung radiation ($\sim$ 20–150 keV x rays) produced as the energetic electrons transit the fuel [24]. Figure 2 shows a plot of the hard-x-ray signal as a function of the peak laser intensity for both $\sim$4-μm-thick CD cryogenic D_2 implosions (open circles) and thick-CH-shell (typically 20–26 μm) gas-filled, room-temperature implosions (solid boxes). The hard-x-ray signal shows the same intensity dependence for both target types; the signal rises exponentially above a threshold and saturates at high intensities. The x-ray production threshold for the thin cryogenic CD shells

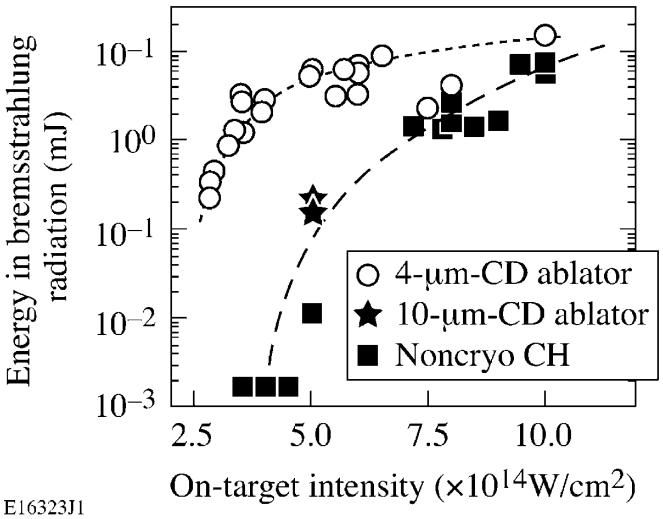

FIG. 2. The measured hard-x-ray signal is plotted as a function of the peak laser-drive intensity for both cryogenic and warm CH-shell implosions. The open circles are from implosions of thin-CD, thick-D_2 cryogenic targets while the solid boxes are from implosions of thick-CH, gas-filled room-temperature targets. The solid stars indicate the hard-x-ray production from the two high ρR_n, thick-CD-shell cryogenic implosions discussed in the text.

is lower than for the thicker warm plastic shells. The laser pulse burns through the thin CD shortly after reaching peak intensity and D_2 becomes the primary ablator. The intensity-threshold difference follows from the high laser absorption in CH (relative to D_2) due to the higher ion charge Z. The enhanced absorption increases the coronal temperature and lowers the laser intensity at the quarter-critical density surface.

Figure 3 shows the correlation between the measured and the predicted ρR_n for a variety of implosion adiabats (diamonds) with thin CD shells and ~95-μm D_2 ice layers [8,13]. The drive intensity ranges from 0.5 to 1×10^{15} W/cm^2, well above the hard-x-ray or hot-electron-production threshold in Fig. 2. The agreement between the measured and the predicted ρR_n is reasonable only for the highest adiabat implosions (i.e., the lowest convergence and most hydrodynamically stable) or the lowest drive intensities (i.e., minimal hot-electron preheat; these points are shown as the open circles in Fig. 3). Measurements of the areal density in noncryogenic, thick-CH-shell implosions agree well with hydrocode simulations when the laser

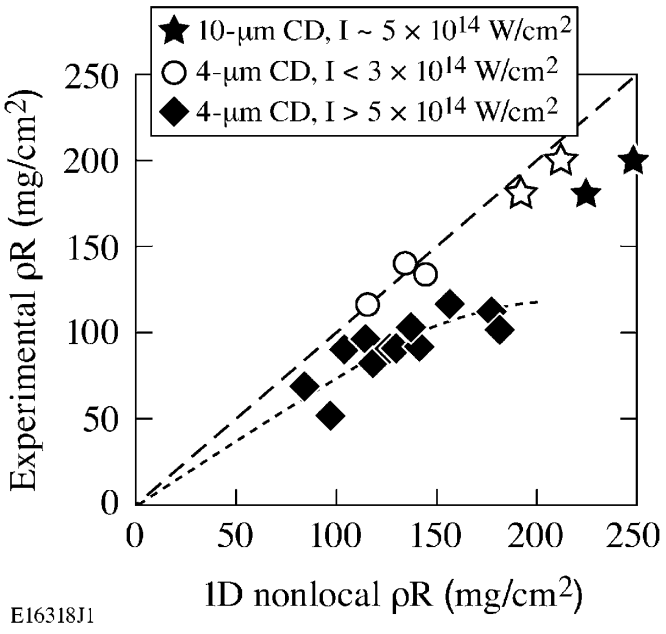

FIG. 3. The measured ρR_n with thin ($\sim$4-μm) CD-shell cryogenic implosions are systematically less than predicted for a range of shell adiabats and drive intensities between 5×10^{14} and 1×10^{15} W/cm^2 (solid diamonds; the dotted line is to emphasize the trend away from the predicted values for lower adiabat implosions where shock timing is not optimized and electron preheat is observed). The agreement with hydrocode predictions improves as the drive intensity is reduced below the threshold for laser-intensity-driven plasma instabilities (open circles). With thicker CD ($\sim$10-μm) ablators, the hot-electron preheat signal is minimized at a drive intensity of 5×10^{14} W/cm^2 and the measured ρR_n agree well with the hydrocode predictions (solid stars; the open stars are corrected for burn truncation as described in the text).

intensity is less than $\sim 6 \times 10^{14}$ W/cm^2 [25]. To prevent D_2 from reaching the quarter-critical surface during the peak laser drive, the thickness of the CD shell was increased to 10 μm. Two of these thicker CD shell capsules (with ~95-μm-thick D_2 ice) were imploded by the drive pulse shown in Fig. 1(b) with the picket intensity and shock timing tuned to minimize shock-induced adiabat degradation. As expected, the hot-electron preheat signal was significantly reduced (the two points are shown in Fig. 2 by the solid stars). For these implosions, the target adiabat was 2.5, the maximum drive intensity was $\sim 5 \times 10^{14}$ W/cm^2, and the inner-ice-surface roughness was 2.3-μm rms in all modes. The ρR_n was inferred from five independent measurements of the secondary-proton spectrum. On shot 47 206, the ρR_n was 202 ± 7 mg/cm^2 (the 1D prediction from LILAC was 247 mg/cm^2). For a second virtually identical target, the picket timing was delayed by 200 ps (with the expectation that the compression wave would steepen into a shock earlier, raising the fuel adiabat and lowering the areal density). For this implosion (shot 47 210), the average of the five measurements was 182 ± 7 mg/cm^2 (the 1D value was 222 mg/cm^2), 10% lower than the properly timed implosion. These two points are shown in Fig. 3 by the solid stars.

Figure 4 shows the average secondary-proton spectra measured on shots 47 206 [Fig. 4(a)] and 47 210 [Fig. 4(b)]. The dashed lines are the normalized sums of the five individual spectra, while the solid curves represent the spectra predicted by LILAC with the proton emission sampling the predicted areal-density distribution according to the experimentally measured neutron-production history (to account for the burn truncated sampling of the experimental ρR evolution discussed above; a thorough review of this technique can be found in Ref. [22]). The predicted neutron-averaged areal density is 212 mg/cm^2 for shot 47 206. The very close agreement between the simulated and measured spectra indicates that the fuel assembly proceeded according to the 1D simulation up to approximately peak density (140 g/cm^3 in the simulation). Similar agreement for shot 47 210 indicates that the deliberate shock mistiming is properly modeled by the simulation. The open stars in Fig. 3 use these burn-weighted predictions; the correction for the lower ρR_n points is approximately 5%, which is within the measurement error. It should be noted that earlier measurements of high-density compression [26] were based on a room-temperature plastic target that does not scale to ignition.

In conclusion, high-density fuel assembly has been successfully demonstrated in cryogenic D_2 implosions on the OMEGA laser at adiabats relevant to the high-gain ignition designs for the NIF. An areal density of 202 ± 7 mg/cm^2 was inferred for an implosion with an adiabat of 2.5. This areal density is 95% of that predicted by hydrodynamic simulations, suggesting that the experimental adiabat was virtually the same as that predicted by the simulation.

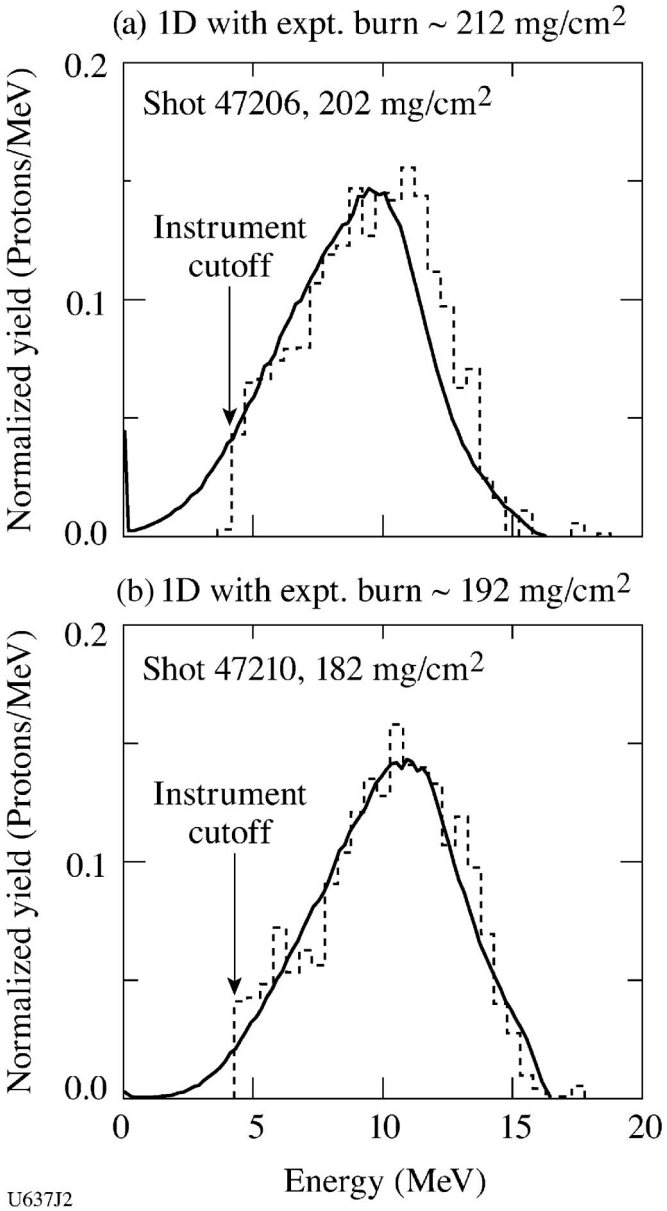

FIG. 4. (a) The average secondary-proton spectrum (dashed histogram) measured for shot 47 206, a thick (10-μm) CD shell with a 95-μm D_2 ice layer. The solid curve represents the spectrum predicted by the 1D simulation. The ρR_n inferred from the measurement is 202 ± 7 mg/cm^2, while the simulated spectrum gives a neutron-averaged value of 212 mg/cm^2. (b) The ρR_n inferred from the measured proton spectrum on shot 47 210 is 182 ± 7 mg/cm^2, while the simulated spectrum gives 192 mg/cm^2.

When the relative timing of the first shock and the compression wave was deliberately changed, the resulting reduction in the measured areal density was accurately predicted by the hydrodynamic simulation. The next step will be to further increase the implosion velocity by thinning the cryogenic fuel layer and driving the shells at higher intensities. Several strategies are being studied to mitigate fast-electron preheat and the growth of perturbations at the ablation surface at the higher intensities. These include high-Z dopants in the plastic ablator and advanced pulse shaping techniques [22]. Based on these high-areal-density measurements and the confidence established in the predictive capability of the design code, prospects for scaling direct-drive target designs to ignition on the NIF are good.

This work was supported by the U.S. Department of Energy Office of Inertial Confinement Fusion under Cooperative Agreement No. DE-FC52-92SF19460, the University of Rochester, and the New York State Energy Research and Development Authority.

*Also at: Departments of Mechanical Engineering and Physics, University of Rochester, Rochester, NY 14623-1299, USA.

[1] J. Nuckolls *et al.*, Nature (London) **239**, 139 (1972).
[2] J. D. Lindl *et al.*, Plasma Phys. Controlled Fusion **45**, A217 (2003).
[3] R. L. McCrory *et al.*, Nucl. Fusion **45**, S283 (2005).
[4] W. J. Hogan *et al.*, Nucl. Fusion **41**, 567 (2001).
[5] J. D. Lindl *et al.*, Phys. Plasmas **11**, 339 (2004).
[6] R. Betti and C. Zhou, Phys. Plasmas **12**, 110702 (2005).
[7] P. W. McKenty *et al.*, Phys. Plasmas **8**, 2315 (2001).
[8] F. J. Marshall *et al.*, Phys. Plasmas **12**, 056302 (2005).
[9] T. C. Sangster *et al.*, Phys. Plasmas **14**, 058101 (2007).
[10] T. R. Boehly *et al.*, Opt. Commun. **133**, 495 (1997).
[11] D. R. Harding *et al.*, Phys. Plasmas **13**, 056316 (2006).
[12] F. H. Séguin *et al.*, Phys. Plasmas **9**, 2725 (2002).
[13] V. A. Smalyuk *et al.*, preceding Letter, Phys. Rev. Lett. **100**, 185005 (2008).
[14] C. S. Liu and M. N. Rosenbluth, Phys. Fluids **19**, 967 (1976).
[15] P. B. Radha *et al.*, Phys. Plasmas **12**, 032702 (2005).
[16] V. N. Goncharov *et al.*, Phys. Plasmas **10**, 1906 (2003).
[17] R. Betti *et al.*, Phys. Plasmas **12**, 042703 (2005).
[18] J. Delettrez *et al.*, Phys. Rev. A **36**, 3926 (1987).
[19] T. R. Boehly *et al.*, Phys. Plasmas **13**, 056303 (2006).
[20] A. Sunahara *et al.*, Phys. Rev. Lett. **91**, 095003 (2003).
[21] V. N. Goncharov *et al.*, Phys. Plasmas **13**, 012702 (2006).
[22] V. N. Goncharov *et al.*, "Performance of Direct-Drive Cryogenic Targets on OMEGA," Phys. Plasmas (to be published).
[23] W. Seka *et al.*, "Laser-Plasma Interaction Processes Observed in Direct-Drive Implosion Experiments," Phys. Plasmas (to be published).
[24] C. Stoeckl *et al.*, Rev. Sci. Instrum. **72**, 1197 (2001).
[25] C. D. Zhou *et al.*, Phys. Rev. Lett. **98**, 025004 (2007).
[26] H. Azechi *et al.*, Laser Part. Beams **9**, 193 (1991).